Full counting statistics of the interference contrast from independent Bose-Einstein condensates

Steffen Patrick Rath and Wilhelm Zwerger
Technische Universität München, Physik Department, James-Franck-Straße, D-85748 Garching, Germany
(Received 24 September 2010; published 19 November 2010)

We show that the visibility in interference experiments with Bose-Einstein condensates is directly related to the condensate fraction. The probability distribution of the contrast over many runs of an interference experiment thus gives the full counting statistics of the condensed atom number. For two-dimensional Bose gases, we discuss the universal behavior of the probability distribution in the superfluid regime and provide analytical expressions for the distributions for both homogeneous and harmonically trapped samples. They are non-Gaussian and unimodal with a variance that is directly related to the superfluid density. In general, the visibility is a self-averaging observable only in the presence of long-range phase coherence. Close to the transition temperature, the visibility distribution reflects the universal order-parameter distribution in the vicinity of the critical point.

DOI: 10.1103/PhysRevA.82.053622 PACS number(s): 03.75.Dg, 37.25.+k

I. INTRODUCTION

Interference experiments constitute an invaluable tool for the characterization of the coherence properties of ultracold gases [1–3]. These properties are particularly intriguing in the case of ultracold one- or two-dimensional (1D or 2D) Bose gases [4–6]. Due to strong phase fluctuations, both the 1D gas at zero temperature and the 2D gas at finite temperature exhibit only quasi-long-range order; that is, the one-body density matrix which measures long-range phase coherence decays as a power law instead of converging to a finite constant for long distances. Due to the quantum nature of the interfering matter fields, the measured visibility is a random variable that differs from one experimental run to another. For the case of 1D Bose gases at zero temperature, the probability distribution of the interference contrast has been calculated analytically for arbitrary strong interactions, using a mapping to the exactly solvable boundary sine-Gordon theory [7]. In the weak coupling limit, it turns out to be a Gumbel distribution [8,9]. Numerical data calculated within the same theoretical framework, but at finite temperature, are in good agreement with experiment [10].

Here we reconsider the issue of the statistics of the interference contrast for Bose-Einstein condensates in arbitrary dimension, discussing in particular the 2D case and the connection between long-range order and self-averaging. We show that the probability distribution of the interference contrast is identical to that of the condensate fraction in the limit of a large integration volume in the absorption images. The resulting distributions therefore provide the precise counting statistics for the number of condensed atoms [11]. The statistics of the condensate number has a universal form in two limiting cases: at the critical point, as a consequence of finite size scaling [12,13], and at temperatures far below the critical temperature. We discuss both cases and give analytical expressions for the distribution for the latter. Specifically, for 2D Bose gases, the distribution at temperatures T far below the critical temperature of the Berezinskii-Kosterlitz-Thouless (BKT) transition [14,15], is controlled by the dimensionless parameter $\eta(T) = 1/n_s\lambda_T^2$, where n_s is the superfluid density, and $\lambda_T = \sqrt{2\pi\hbar^2/mk_BT}$ the thermal wavelength. The fluctuations around the average visibility are determined by the superfluid density, a quantity that is rather difficult to measure by other means [16]. For a homogeneous square sample, we show that the probability distribution of the interference contrast is close to a convolution of two Gumbel distributions, similar to but different from the Gumbel distribution that is obtained for the weakly interacting limit of a 1D Bose gas at zero temperature [8,9]. Non-Gaussian distributions are also found in harmonically trapped and strongly anisotropic 2D gases, in qualitative agreement with preliminary data taken at the Ecole normale supérieure (ENS) in Paris [17]. The principal focus of this article is on the physics of 2D Bose gases, but we highlight the differences and similarities to the 3D case as well as the 1D case at vanishing temperature.

This article is organized as follows. In Sec. II, we introduce the physical system and discuss the connection between the measured distribution of the interference contrast and that of the condensed fraction. In Sec. III we use a functional integral description for explicit analytical or numerical calculations of the visibility distribution in the regime where phase fluctuations are dominant. In particular, we discuss the general form of the probability distribution in terms of its cumulants and the issue of self-averaging. Section IV is devoted to the explicit analytical calculation of the probability distribution in the 2D case far below the BKT transition temperature for both a homogeneous system and a harmonically trapped sample. In Sec. V, we discuss the scaling behavior of the probability distribution of the interference contrast at the critical point, where the average visibility vanishes. The 1D case and the anomalous fluctuations of the condensate fraction in 3D are discussed in the appendices.

II. INTERFERENCE STATISTICS

Typical interference experiments with 2D Bose gases (e.g., [2,18]) start out by preparing a pair of such gases confined to the lowest transverse mode in the z direction and separated by a distance d in the z direction. The atoms are then released from the trap and imaged after an adjustable free expansion time using absorption imaging (time-of-flight measurement). When the trapping potentials are cut off, the gases rapidly expand in the z direction while the density distribution as a function of x and y can approximately be regarded as constant. Within this initial expansion period, there is no transformation of phase

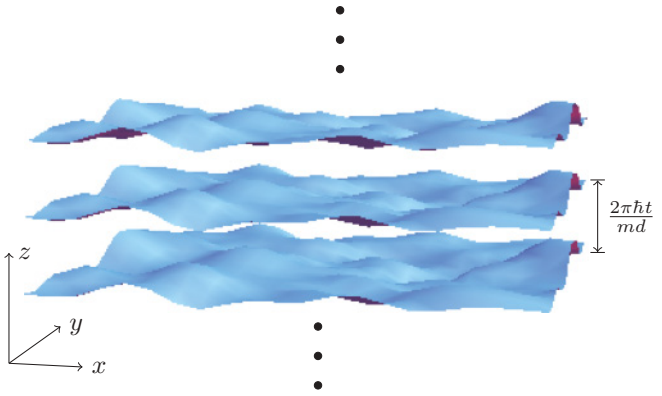

FIG. 1. (Color online) Illustration of the experimental situation in the 2D case. After a time t of rapid expansion, two identical Bose gases overlap and interfere. The interference pattern is characterized by its iso-phase surfaces. Three surfaces having all the same phase are shown for illustration, the pattern itself continues all over the vertical extension of the sample, as suggested by the continuation dots above and below the shown surfaces. The sample is imaged using an absorption beam in the y direction.

fluctuations into density fluctuations, which only sets in at a later stage [19]. Due to the rapid expansion along z, the gases completely overlap after a time t of the order of 20 ms for typical traps. The difference between their phases then results in a spatially modulated interference pattern (see Fig. 1).

The operator for the atomic density after time of flight at an observation point $\boldsymbol{x}$ can be written as [20]

$$\hat{n}(\boldsymbol{x}) = n_0(z)[\hat{n}_1(\boldsymbol{r}) + \hat{n}_2(\boldsymbol{r}) + \hat{A}(\boldsymbol{r})e^{iQz} + \text{H.c.}]. \tag{1}$$

Here $n_0(z)$ is an envelope function (i.e., a normalized function of z which has a negligible Fourier component at the wave number Q of the expansion), $\hat{n}_{1,2}$ are the *in situ* (i.e., before time of flight) density operators of the individual gases, $Q = md/\hbar t$ is the wave vector associated with the ballistic expansion, and $\hat{A}(\boldsymbol{r}) = \hat{\psi}_1^\dagger(\boldsymbol{r})\hat{\psi}_2(\boldsymbol{r})$ is the operator that determines the local interference amplitude. Here and in the following, we use $\boldsymbol{r}$ to denote a point in the trap before time of flight and $\boldsymbol{x}$ for observation points after time of flight [6].

In a given experimental run, the measured density distribution $n(\boldsymbol{x})$ corresponds to an eigenstate of the Hermitian operator $\hat{n}(\boldsymbol{x})$ and $\hat{A}(\boldsymbol{r})$ can be replaced by a complex number $A = \mathcal{V}(\boldsymbol{r})e^{i\phi(\boldsymbol{r})}$. The resulting density can then be written in the standard form $n_0(\boldsymbol{x})(1 + \mathcal{V}(\boldsymbol{r})\cos\{Q[z - z_0(\boldsymbol{r})]\})$ of an interference pattern with the local visibility $\mathcal{V}(\boldsymbol{r}) = |A|$ and a spatially varying shift $z_0(\boldsymbol{r}) = -\phi(\boldsymbol{r})/Q$. When the interference pattern is integrated over a finite volume, spatial variations of both $\mathcal{V}(\boldsymbol{r})$ (caused by density fluctuations) and $z_0(\boldsymbol{r})$ (caused by phase fluctuations) lead to a reduction of the integrated visibility $\mathcal{V}$. The height function z_0 defines a surface in real space, the iso-phase surface. In 1D or 2D, there is one unique iso-phase surface which is repeated over the entire extension of the sample (cf. Fig. 1). In 3D, z_0 depends on all three spatial coordinates and the shape of the iso-phase surfaces is different for different phase values. Provided that density fluctuations are negligible, which is always the case in the strongly degenerate regime [21], the integrated interference contrast is completely determined by the shape of the iso-phase surfaces.

The interference amplitude in a given run of the experiment can be extracted from the measured density $n(\boldsymbol{x})$ by taking the Fourier transform along z and evaluating it at the wave vector Q, where the magnitude of the local interference amplitude,

$$A_Q(x,y) = \int dz n(\boldsymbol{x})e^{-iQz}, \tag{2}$$

takes its maximum. This yields a complex number which contains the random relative phase between the two clouds. Its average over many runs will therefore vanish. Here we are interested in the modulus square of A_Q, which determines the observed visibility of the interference fringes. Experimentally, the local amplitude $|A_Q(x,y)|^2$ is not a directly accessible quantity since the absorption imaging automatically integrates over the y direction. In practice, the averaged interference contrast is obtained by extending the domain of integration over a volume Ω that typically covers the entire sample. It is then convenient to define an operator,

$$\hat{\alpha} = \int_\Omega d^3x \int_\Omega d^3x' \hat{n}(\boldsymbol{x})\hat{n}(\boldsymbol{x}')e^{-iQ(z-z')}, \tag{3}$$

whose eigenvalues represent the magnitude of the integrated contrast in an individual run [20]. In terms of the basic in-trap field operators, this operator can be expressed by

$$\hat{\alpha} = \int_\Omega d^d r d^d r' \hat{\psi}_1^\dagger(\boldsymbol{r})\hat{\psi}_1(\boldsymbol{r}')\hat{\psi}_2(\boldsymbol{r})\hat{\psi}_2^\dagger(\boldsymbol{r}'). \tag{4}$$

Now, in a homogeneous condensate, the one-body density matrix $\hat{\psi}_i^\dagger(\boldsymbol{r})\hat{\psi}_i(\boldsymbol{r}')$ approaches a constant on length scales $|\boldsymbol{r} - \boldsymbol{r}'|$ larger than the healing length. Moreover, one has $\hat{\psi}_2(\boldsymbol{r})\hat{\psi}_2^\dagger(\boldsymbol{r}') \approx \hat{\psi}_2^\dagger(\boldsymbol{r}')\hat{\psi}_2(\boldsymbol{r})$ up to corrections that vanish like $1/\Omega$. As a result, the operator

$$\hat{\alpha} \simeq \Omega^{-2}\left(\int d^d r d^d r' \hat{\psi}_1^\dagger(\boldsymbol{r})\hat{\psi}_1(\boldsymbol{r}')\right) \times \left(\int d^d r d^d r' \hat{\psi}_2^\dagger(\boldsymbol{r})\hat{\psi}_2(\boldsymbol{r}')\right) = \hat{N}_0^{(1)}\hat{N}_0^{(2)}, \tag{5}$$

whose eigenvalues determine the measured interference contrast in a given run, is equal to the product of the number of condensed atoms,

$$\hat{N}_0^{(i)} = \Omega^{-1}\int d^d r d^d r' \hat{\psi}_i^\dagger(\boldsymbol{r})\hat{\psi}_i(\boldsymbol{r}'), \tag{6}$$

within the integration volume Ω of each initial condensate. It is important to emphasize that this argument does not rely on the presence of true long-range phase coherence. In particular, it is valid for 2D Bose gases at finite and 1D Bose gases at zero temperature, where the one particle density matrix approaches a finite value $\tilde{n}_0$ on scales much larger than the interparticle spacing. The eventual algebraic decay to zero only appears at distances beyond a phase coherence length ℓ_ϕ that is still much larger. For an integration volume that contains a large number of particles $N \gg 1$ and identically prepared samples, therefore, the operator $\hat{\alpha}$ is just the square of the condensed atom number in each sample. The eigenvalues α of $\hat{\alpha}$, which are the experimental observables according to the standard rules of quantum mechanics, thus may take any value between zero and N^2, where N is the number of atoms in either of the two samples. The measured integrated density as a function of

z varies between $2N - 2\sqrt{\alpha}$ and $2N + 2\sqrt{\alpha}$. The visibility $\mathcal{V}$ is therefore simply $\sqrt{\alpha}/N$, or

$$\mathcal{V}^2 = \frac{\alpha}{N^2} = \left(\frac{N_0}{N}\right)^2. \tag{7}$$

The measured distribution of the visibility thus directly reflects that of the condensate fraction.

Our aim in the following is to calculate the probability distribution for the different positive eigenvalues α of $\hat{\alpha}$. For a given many-body state characterized by a density operator $\hat{\rho}$, the associated probability distribution is just $p(\alpha) = \langle\alpha|\hat{\rho}|\alpha\rangle$. Mathematically, it is more convenient to calculate its characteristic function

$$p(\sigma) \equiv \int_{-\infty}^{\infty} d\alpha\, p(\alpha) e^{i\sigma\alpha} = \mathrm{Tr}[\hat{\rho} e^{i\sigma\hat{\alpha}}] = \langle e^{i\sigma\hat{\alpha}}\rangle. \tag{8}$$

To proceed further, we replace $e^{i\sigma\hat{\alpha}}$ with its normal-ordered counterpart $:e^{i\sigma\hat{\alpha}}:$. This approximation neglects commutator terms which describe the effect of atomic shot noise [22] and are of relative order $1/N$ [8]. Since typical integration volumes for a measurement of the interference contrast contain $N \sim 10^3$ atoms at least, this approximation is valid up to corrections of less than 1% . A convenient representation for the calculation of the characteristic function (8) is obtained by evaluating the trace in terms of coherent states. This gives rise to a functional integral,

$$p(\sigma) = (\mathcal{N}_1\mathcal{N}_2)^{-1} \int \mathcal{D}(\bar{\psi}_1,\psi_1)\mathcal{D}(\bar{\psi}_2,\psi_2) e^{-S_1[\bar{\psi}_1,\psi_1]-S_2[\bar{\psi}_2,\psi_2]} \times \exp\left[i\sigma \left|\int d^d r \bar{\psi}_1(\boldsymbol{r})\psi_2(\boldsymbol{r})\right|^2\right], \tag{9}$$

over bosonic c-number fields $\psi(\boldsymbol{r},\tau)$, which are periodic in the interval $\tau = [0,\beta]$. (Here and in the following, we adopt units in which $\hbar = k_B = 1$.) Here $S_{1,2}$ are the respective actions for the interacting Bose gases 1,2, while $\mathcal{N}_i = \int \mathcal{D}(\bar{\psi}_i,\psi_i)\exp(-S_i[\bar{\psi}_i,\psi_i])$ are normalization factors. Due to our normal-ordering approximation, the fields in the last exponential do not vary with τ, in contrast to the fields appearing in the action, but are evaluated at $\tau = 0$. For notational simplicity, $\psi_i(\boldsymbol{r},0) \equiv \psi_i(\boldsymbol{r})$. By a simple redefinition of $\sigma \to \sigma/N^2$, Eq. (9) gives the characteristic function for the square $\mathcal{V}^2$ of the visibility, which is a direct measure of the interference contrast.

Within the functional integral, it is convenient to switch to the density-phase representation $\psi_i(\boldsymbol{r}) = \sqrt{n_i(\boldsymbol{r})}e^{i\varphi_i(\boldsymbol{r})}$ for the c-number fields. In this representation, the square of the visibility $\mathcal{V}^2$ reads

$$\begin{aligned}\mathcal{V}^2 &= \frac{1}{N^2}\int d^d r d^d r' \bar{\psi}_1(\boldsymbol{r})\psi_1(\boldsymbol{r}')\psi_2(\boldsymbol{r})\bar{\psi}_2(\boldsymbol{r}') \\ &= \frac{1}{N^2}\int d^d r d^d r' \sqrt{n_1(\boldsymbol{r})n_1(\boldsymbol{r}')n_2(\boldsymbol{r})n_2(\boldsymbol{r}')} \\ &\quad \times e^{i\{[\varphi_2(\boldsymbol{r})-\varphi_1(\boldsymbol{r})]-[\varphi_2(\boldsymbol{r}')-\varphi_1(\boldsymbol{r}')]\}}.\end{aligned} \tag{10}$$

In particular, for temperatures low enough that the influence of density fluctuations around an average $\bar{n}(\boldsymbol{r})$ may be neglected, the visibility

$$\mathcal{V}^2 \approx \left|\frac{1}{N}\int d^d r \bar{n}(\boldsymbol{r}) e^{i[\varphi_2(r)-\varphi_1(r)]}\right|^2 \tag{11}$$

only depends on the phase difference $\phi \equiv \varphi_2 - \varphi_1$.

III. INTERFERENCE CONTRAST AT LOW TEMPERATURE

In the following, we assume that the two gases are identical and describe each one using the quantum hydrodynamic action

$$S[\varphi_j] = \int_0^\beta d\tau \int d^d r \left\{\frac{n_s(\boldsymbol{r})}{2m}[\nabla\varphi_j(\boldsymbol{r},\tau)]^2 + \frac{1}{2g}[\partial_\tau\varphi_j(\boldsymbol{r},\tau)]^2\right\}. \tag{12}$$

Here $\beta = 1/T$ is the inverse temperature, m is the atomic mass, and g is a coupling constant, which is just the inverse of the compressibility κ. Moreover, n_s is the superfluid density, which is inhomogeneous in trapped gases. The action (12) provides a completely general low-energy description of superfluid Bose gases. In particular, it describes 3D gases below the critical temperature for Bose-Einstein condensation, 2D gases below the BKT transition [14,15], and 1D gases at zero temperature.

Since $\mathcal{V}^2$ depends only on the phase difference, it is advantageous to switch to a new set of variables:

$$\Phi = \frac{\varphi_2 + \varphi_1}{2}; \quad \phi = \varphi_2 - \varphi_1. \tag{13}$$

In terms of these variables, the total action can be rearranged as

$$S = S[\varphi_1] + S[\varphi_2] = 2S[\Phi] + \tfrac{1}{2}S[\phi], \tag{14}$$

which implies that the contribution depending on the total average phase Φ cancels out in Eq. (9). The characteristic function (9) can then be written as

$$p(\sigma) = \frac{1}{\mathcal{N}}\int \mathcal{D}\phi e^{-S[\phi]/2} \exp\left[i\sigma\left|\int \frac{d^d r}{N}\bar{n}(\boldsymbol{r})e^{i\phi(\boldsymbol{r})}\right|^2\right], \tag{15}$$

with $\mathcal{N} = \int \mathcal{D}\phi \exp(-S[\phi]/2)$. Note that a constant contribution in ϕ has no effect on the result since it cancels out when taking the modulus square. In the following, we thus restrict our analysis to functions without constant component, that is, $\int d^d r\phi(\boldsymbol{r}) = 0$.

For explicit calculations, we follow the technique used by Imambekov *et al.* [8,9] and parametrize the functional integral (15) by expanding ϕ in terms of the solutions of the imaginary time Euler-Lagrange equation associated with the action (12),

$$\partial_\tau^2\phi(\boldsymbol{r},\tau) + \frac{g}{m}\nabla\cdot[n_s(\boldsymbol{r})\nabla\phi(\boldsymbol{r},\tau)] = 0, \tag{16}$$

supplemented with appropriate spatial boundary conditions. The bosonic nature of the field $\phi(\boldsymbol{r},\tau)$ requires that the solutions satisfy $\phi(\boldsymbol{r},0) = \phi(\boldsymbol{r},\beta)$. A separation ansatz readily gives a family of solutions $\psi_\lambda(\boldsymbol{r})e^{\pm\omega_\lambda\tau}$, where λ is a formal

index labeling the eigenmodes. To satisfy the boundary condition on τ, we use the expansion

$$\phi(\boldsymbol{r},\tau)=\sum_{\lambda\neq 0}s_\lambda\psi_\lambda(\boldsymbol{r})\left(\frac{e^{\omega_\lambda\tau}}{e^{\beta\omega_\lambda}+1}+\frac{e^{\beta\omega_\lambda}e^{-\omega_\lambda\tau}}{e^{\beta\omega_\lambda}+1}\right). \tag{17}$$

Factors have been chosen so that the parentheses evaluate to unity at $\tau=0$ and $\tau=\beta$.

Unless excluded by the boundary conditions, the Euler-Lagrange equation always permits a solution $\psi_0(\boldsymbol{r})$ which is constant and nonzero in space. Since the modes ψ_λ form a complete orthonormal system, $\int d^dr\,\psi_\lambda(\boldsymbol{r})\psi_{\lambda'}(\boldsymbol{r})=\delta_{\lambda,\lambda'}$, this implies that all further modes have a vanishing spatial average. The condition $\int d^dr\,\phi=0$ therefore translates to the omission of the constant mode $\lambda=0$.

Substituting the expansion (17) into the action yields a diagonal quadratic form

$$\frac{S}{2}=\sum_{\lambda\neq 0}\frac{s_\lambda^2}{2g}\omega_\lambda\tanh\left(\frac{\beta\omega_\lambda}{2}\right). \tag{18}$$

Introducing the dimensionless variables

$$t_\lambda\equiv s_\lambda\sqrt{\frac{\omega_\lambda}{g}\tanh\left(\frac{\beta\omega_\lambda}{2}\right)}, \tag{19}$$

the characteristic function can then be rewritten as

$$p(\sigma)=\prod_{\lambda\neq 0}\int\frac{dt_\lambda e^{-\frac{t_\lambda^2}{2}}}{\sqrt{2\pi}}\exp\left(i\sigma\left|\int\frac{d^dr}{N}\bar{n}(\boldsymbol{r})e^{ih_{\{t_\lambda\}}(r)}\right|^2\right), \tag{20}$$

where

$$h_{\{t_\lambda\}}(\boldsymbol{r})=\phi(\boldsymbol{r},0)=\sum_{\lambda\neq 0}\sqrt{\frac{g}{\omega_\lambda}\coth\left(\frac{\beta\omega_\lambda}{2}\right)}t_\lambda\psi_\lambda(\boldsymbol{r}) \tag{21}$$

is the parametrized iso-phase surface. This expression has already been derived by Imambekov *et al.* [9], starting from the relationship between the moments of $\mathcal{V}^2$ and higher-order correlation functions. The fluctuating surface h emerged as an abstraction in their article. Here we see that it is just the shape of the iso-phase surfaces.

Equations (20) (or rather, the expression for $\mathcal{V}^2$ appearing therein) and (21) are well suited for numerical use: To obtain a given realization of $\mathcal{V}^2$, one generates a large number of Gaussian deviates for the amplitudes t_λ, constructs the corresponding surface h, and numerically calculates the integral to obtain $\mathcal{V}^2$. Repeating this sequence with different sets of amplitudes yields histograms for the possible values of $\mathcal{V}^2$, whose shape approaches the actual probability distribution as the number of iterations grows large.

Analytical results can be obtained in the limit of high contrasts, $1-\mathcal{V}^2\ll 1$, where the iso-phase surfaces are smooth and one may expand the exponential inside the definition of $\mathcal{V}^2$. As is clear from Eq. (21), the expansion parameter is given by

$$\epsilon\equiv\max_{\lambda,\boldsymbol{r}}\sqrt{\frac{g}{\omega_\lambda}\coth\left(\frac{\beta\omega_\lambda}{2}\right)}\psi_\lambda(\boldsymbol{r}). \tag{22}$$

In all cases that we encounter in the following, this maximum is found for $\omega_{\min}\equiv\min_{\lambda\neq 0}\omega_\lambda$.

In the following, we focus on the regime where the reduction of the visibility is dominated by thermal fluctuations so that quantum fluctuations (caused by interactions) may be neglected. Considering, in particular, a 2D Bose gas whose characteristic size l_z in the direction of transverse confinement obeys $l_z\gg a_s$, the effect of zero point fluctuations of the phase on the reduction of the visibility can be determined by a Bogoliubov calculation, which gives [21]

$$\langle\mathcal{V}^2\rangle(T=0)=\left(\frac{n_0(0)}{n}\right)^2=1-\frac{\tilde{g}_2}{2\pi}+\cdots. \tag{23}$$

Here, $\tilde{g}_2=mg_2=\sqrt{8\pi}a_s/l_z$ is the dimensionless 2D interaction constant, which has typical values $\tilde{g}_2=0.1$ [2,17], which implies practically unit visibility at zero temperature. By contrast, at finite temperature, the integrated visibility

$$\langle\mathcal{V}^2\rangle(T)-\langle\mathcal{V}^2\rangle(0)=\left[1-2\eta(T)\log\left(\frac{L}{\xi}\right)\right] \tag{24}$$

decreases logarithmically with the size of the system, which reflects the absence of long-range order at finite temperature in the thermodynamic limit [23,24]. Since the size dependence of the thermal depletion is only logarithmic, finite condensate fractions may be found at low-enough temperature for realistic system sizes.

In actual experiments, the temperature is usually large compared to the typical frequencies ω_λ, which are of the order of the chemical potential μ. Then $\coth(\beta\omega_\lambda/2)$ can be replaced with $2T/\omega_\lambda$ and hence $\epsilon^2=2gT\max_{\lambda,\boldsymbol{r}}\psi_\lambda(\boldsymbol{r})^2/\omega_\lambda^2$. Within this approximation the effect of thermal phase fluctuations scales linearly with temperature. For weakly interacting 2D Bose gases, the necessary condition $T\gg\mu$ is well obeyed even in the deeply degenerate regime because $\mu/T=\tilde{g}_2/2\pi$ at $n\lambda_T^2=\mathcal{O}(1)$ [6]. Note that for $\tilde{g}_2\ll 1$ the conditions $T\gg\mu$ and $\epsilon^2\ll 1$ are simultaneously satisfied for the typical phase-space densities $n\lambda_T^2$ that are reached in 2D Bose gases [25].

Quite generally, whether or not ϵ is small, that is, whether a physical regime which permits such an expansion exists, depends crucially on temperature and the spatial dimension d. Because of normalization, the eigenfunctions ψ_λ scale with the characteristic size $L=\Omega^{1/d}$ of the system as $L^{-d/2}$, while the eigenfrequencies ω_λ will scale as L^{-1}, independent of the dimensionality. It follows that ϵ scales as $L^{1-d/2}$. For concreteness, in a homogeneous system with periodic boundary conditions,

$$\epsilon^2=\frac{L^{2-d}}{\pi^2}\frac{mT}{n_s}. \tag{25}$$

For the case of 2D Bose gases, which is the main focus of our work, $\epsilon^2=2\eta(T)/\pi$ is independent of system size and is determined by the exponent $\eta(T)=(n_s\lambda_T^2)^{-1}$, which gives the decay of the one-body density matrix.

For $\epsilon\ll 1$, the exponent in Eq. (20) can be expanded in the form

$$\exp\left(i\sum_{\lambda\neq 0}\epsilon t_\lambda\right)\simeq 1+i\sum_{\lambda\neq 0}\epsilon t_\lambda-\frac{1}{2}\sum_{\lambda,\lambda'\neq 0}\epsilon^2 t_\lambda t_{\lambda'}, \tag{26}$$

since the variables t_λ are of order one due to the Gaussian weight factors $e^{-t_\lambda^2/2}$. Within this approximation, an exact calculation of the distribution functions is possible. The inclusion of the terms quadratic in ϵ leads to nontrivial distributions instead of the Delta functions that result in leading order in ϵ [8]. In the general case of an inhomogeneous system with a spatially varying superfluid density $n_s(\boldsymbol{r})$, thermal phase fluctuations lead to a reduction of the visibility from unity (or—more precisely—from its value at zero temperature) of the form

$$1-\mathcal{V}^2=\frac{2gT}{\Omega}\left[\sum_{\lambda,\lambda'\neq 0}\frac{t_\lambda t_{\lambda'}}{\omega_\lambda\omega_{\lambda'}}I_{\lambda,\lambda'}-\left(\sum_{\lambda\neq 0}\frac{t_\lambda}{\omega_\lambda}J_\lambda\right)^2\right], \quad (27)$$

where Ω is the integration volume and

$$I_{\lambda,\lambda'}=\frac{\Omega}{N}\int d^dr\bar{n}(\boldsymbol{r})\psi_\lambda(\boldsymbol{r})\psi_{\lambda'}(\boldsymbol{r}),$$
$$J_\lambda=\frac{\sqrt{\Omega}}{N}\int d^dr\bar{n}(\boldsymbol{r})\psi_\lambda(\boldsymbol{r}) \quad (28)$$

are dimensionless numbers. In a homogeneous system, $I_{\lambda,\lambda'}=\delta_{\lambda,\lambda'}$, and $J_\lambda=0$ for any λ. In inhomogeneous systems, there may be finite "off-diagonal" values for $I_{\lambda,\lambda'}$ and finite values for J_λ.

For a discussion of some general features of the statistics of the interference contrast like the dependence on dimensionality and the related issue of self-averaging, we focus on homogeneous systems (we discuss the experimentally relevant trapped 2D system in Sec. IV C). It is then convenient to define

$$u\equiv\frac{2}{\epsilon^2}(1-\mathcal{V}^2)=\sum_{\lambda\neq 0}\frac{t_\lambda^2}{\tilde{\omega}_\lambda^2}, \quad (29)$$

where ϵ^2 has been defined in Eq. (25) and $\tilde{\omega}_\lambda\equiv\omega_\lambda/\omega_{\min}$. Note that the scaling factor $2/\epsilon^2$ between $1-\mathcal{V}^2$ and u is large compared to one. While the visibility takes values on the interval $[0,1]$, the auxiliary variable u has values on the interval $[0,\infty]$ due to our expansion of $e^{i\phi(r)}$. The characteristic function

$$q(\sigma)=\langle e^{i\sigma u}\rangle=\int\prod_{\lambda\neq 0}\frac{dt_\lambda e^{-t_\lambda^2/2}}{\sqrt{2\pi}}\exp\left(i\sigma\sum_{\lambda\neq 0}\frac{t_\lambda^2}{\tilde{\omega}_\lambda^2}\right) \quad (30)$$

of the probability distribution $q(u)$ for the rescaled deviation u of the visibility from unity is now readily evaluated to be

$$q(\sigma)=\prod_{\lambda\neq 0}\frac{1}{\sqrt{1-2i\sigma/\tilde{\omega}_\lambda^2}}. \quad (31)$$

This evaluation ceases to be straightforward when $I_{\lambda,\lambda'}$ is not diagonal, since it amounts to the calculation of the determinant of an infinite matrix with a nontrivial entry structure.

The logarithm

$$\log q(\sigma)=\frac{1}{2}\sum_{s=1}^{\infty}\frac{(2i\sigma)^s}{s}\zeta_{\{\lambda\}}(s)=\sum_{s=1}^{\infty}\frac{(i\sigma)^s}{s!}\langle u^s\rangle_c \quad (32)$$

of the characteristic function $q(\sigma)$, which is the generating function of the cumulants of u, can be expressed in terms of the spectral ζ function $\zeta_{\{\lambda\}}(s)\equiv\sum_{\lambda\neq 0}(\tilde{\omega}_\lambda^2)^{-s}$ of the eigenfrequencies of the quantum hydrodynamic action (12). In particular, it determines all cumulants of the random variable u via

$$\langle u^s\rangle_c=2^{s-1}(s-1)!\zeta_{\{\lambda\}}(s). \quad (33)$$

Note that this calculation does not depend on the explicit form of the eigenvalues and eigenfunctions: The geometry of the system is completely contained in the factor between u and $1-\mathcal{V}^2$ and the spectral ζ function (for systems with diagonal $I_{\lambda,\lambda'}$).

The precise form of the spectral ζ function obviously depends on the geometry of the system and the spectrum that follows from it, but the following properties are valid for any homogeneous system: $\zeta_{\{\lambda\}}(s)$ is a monotonically decreasing function of its argument and has a lower bound (which is reached in the limit $s\to\infty$) equal to the degeneracy of $\omega_{\min}$ (note that this essential property cannot be reproduced when one replaces the sum in $\zeta_{\{\lambda\}}(s)$ with an integral). It follows that for increasing s, the number of frequencies that make a non-negligible contribution to the value of $\zeta_{\{\lambda\}}(s)$ decreases so that higher-order cumulants will essentially depend only on a small number of low frequencies. However, we find that it diverges for $s=1$ in $d\geqslant 2$ and must be rendered finite by the introduction of a UV cutoff.

Substituting back from Eq. (29), we obtain the cumulants of $\mathcal{V}^2-1$ (which are identical to the cumulants of $\mathcal{V}^2$ except for the expectation):

$$\langle(\mathcal{V}^2-1)^s\rangle_c=\frac{(s-1)!}{2}(-\epsilon^2)^s\zeta_{\{\lambda\}}(s). \quad (34)$$

As will be shown in Eq. (35) below, the spectral ζ function remains finite for all $s\geqslant 2$ in all relevant cases, thus determining the finite size scaling behavior of all higher cumulants: In d dimensions, the sth cumulant scales as $L^{s(2-d)}$.

Specifically, we consider a homogeneous system in d dimensions in a hypercubic volume $\Omega=L^d$ with periodic boundary conditions. Then, $\omega_{\boldsymbol{k}}=c|\boldsymbol{k}|$, with $\boldsymbol{k}=(2\pi/L)(l_1,\ldots,l_d)$, where $l_i\in\mathbb{Z}$, and the speed of sound $c=\sqrt{gn_s/m}$. The resulting spectral ζ function then reads

$$\zeta_{\{\boldsymbol{k}\}}(s)=\sum_{l_1,\ldots,l_d}{}'\frac{1}{\left(l_1^2+\cdots+l_d^2\right)^s}=\sum_{n=1}^{\infty}A_d(n)\frac{1}{n^s}, \quad (35)$$

where the prime on the sum indicates that the point $l_1=\cdots=l_d=0$ is omitted and $A_d(n)$ is the number of possibilities to represent the integer n as a sum of d squares (including squares of negative numbers). The representation on the right-hand side is a special case of a Dirichlet series which arises in connections between number-theory and modular forms [26].

The expectation is then given by Eqs. (34) and (35) with $s=1$. However, simple power counting reveals that the spectral ζ function is UV divergent at $s=1$ in 2D and 3D. Since the quantum hydrodynamic action (12) is an effective low-energy description, however, this divergence is an artifact. It can be avoided by introducing a cutoff at a maximum momentum $\Lambda=2\pi/\xi$, where ξ is the healing length. The necessity of an explicit UV cutoff has the important consequence that the expectation does not follow the scaling with system size announced in Eq. (34): in 2D, the cutoff introduces a logarithmic dependence on system size that would otherwise

be absent so that the expectation takes on a nonuniversal character. During the remainder of this article, we focus on the higher cumulants (from the variance on), which are universal.

Since the variance is independent of system size (as are all higher cumulants) while the expectation vanishes logarithmically as $L \to \infty$, fluctuations are not self-averaging in 2D and the regime $1 - \mathcal{V}^2 \ll 1$ can only be reached in finite-size systems (even if they may in fact be quite large due to the weak logarithmic size dependence of the expectation). This is in contrast to the 3D situation, where as a consequence of true long-range order, the expectation is finite in the thermodynamic limit while all higher cumulants decrease with increasing system size. In this case, the visibility is a self-averaging observable, that is, for large integration volumes Ω, the value obtained in a single run is equal to an average over many runs. In Sec. IV, we focus on system sizes where the condensate depletion remains small and the visibility is close to unity, that is, $L \ll \ell_\phi = \xi e^{1/2\eta(T)}$, and the system is a true condensate rather than a quasicondensate [21]. The opposite case is discussed in Sec. V.

The fact that all cumulants from the variance on are finite and obey the scaling given in Eq. (34) implies that the probability distribution $p(\mathcal{V}^2)$ is universal and non-Gaussian. The following section is devoted to the explicit analytic calculation of this distribution in different geometries.

IV. ANALYTICAL RESULTS IN 2D

For a given geometry and boundary conditions, one can always evaluate the spectral ζ function numerically. Equation (34) then permits the calculation of an arbitrary number of cumulants. However, this is not sufficient to obtain an analytical expression for the underlying probability distribution $p(\mathcal{V}^2)$, which requires a closed-form expression for $\zeta_{\{\lambda\}}(s)$. This may be obtained in the 2D case for simple geometries, which we discuss in this section.

In order to clarify the applicability of our results to experiment, it is necessary to define what we mean by "2D" in practice. We consider the two gases to be strongly confined along the z direction with a trapping potential ω_z which is sufficiently strong to ensure $\omega_z \gg T$ and $\omega_z \gg \mu$ so that the gases reside in the harmonic oscillator ground state along the z direction. However, the spatial extension $l_z = \sqrt{1/m\omega_z}$ shall still be large compared to the scattering length a_s. This regime, which is sometimes referred to as "quasi-2D" [27], accurately describes the situation in typical experiments on cold atoms where the tight confinement is realized using an optical dipole potential [2,18,28–31]. It is particularly simple in that the interaction may be described by a simple dimensionless constant $\tilde{g} = mg = \sqrt{8\pi} a_s / l_z$ (for not too strong interactions. Here and in the following, we drop the subscript "2" for ease of notation), whereas the interaction constant in a 2D system with $l_z \lesssim a_s$ depends on the chemical potential and thus effectively on the spatial density [27].

The first case we discuss is that of a rectangle with periodic boundary conditions. The latter are certainly artificial, but the results are important from a conceptual point of view because the calculation can be carried out in closed form. We discuss two limiting cases of this particular case (isotropic and strongly anisotropic) before moving on to the experimentally relevant case of a harmonically trapped sample.

A. Homogeneous square sample

The conceptually and mathematically most elementary case is the one where the gas is homogeneous and confined to a rectangular area of extension $L \times aL$, $0 < a \leqslant 1$, with periodic boundary conditions. First, we focus on the particular case $a = 1$, that is, a square sample, but it is convenient to introduce the notation directly in its slightly more general form for arbitrary a. In this case, the eigenfunctions take the simple form

$$\psi_k^{(c)} = \sqrt{\frac{2}{aL^2}} \cos(\boldsymbol{k} \cdot \boldsymbol{r}); \quad \psi_k^{(s)} = \sqrt{\frac{2}{aL^2}} \sin(\boldsymbol{k} \cdot \boldsymbol{r}), \tag{36}$$

with $\boldsymbol{k} = (2\pi/L) \times (n_1/a, n_2)$ and $n_{1,2} \in \mathbb{Z}$.

We may now give an explicit expression for the expansion parameter ϵ defined in Eq. (22) and the relationship between $\mathcal{V}^2$ and the auxiliary variable u. For this particular set of eigenfunctions and eigenvalues,

$$\epsilon^2 = \frac{1}{a\pi^2} \frac{mT}{n_s} = \frac{2}{\pi a} \eta(T); \quad u = \frac{2}{\epsilon^2}(1 - \mathcal{V}^2). \tag{37}$$

Quite remarkably, ϵ and hence the entire probability distribution $p(\mathcal{V}^2)$ have no explicit dependence on the interaction constant g, which is hidden in the nontrivial relation between the superfluid density that enters $\eta(T)$ and the bare 2D density n. For weakly interacting Bose gases, this relation has been worked out in [32].

As we already stated, the calculation of a closed-form expression for the probability distribution $p(\mathcal{V}^2)$ requires a closed-form expression for $\zeta_{\{\boldsymbol{k}\}}^{(a)}$. It turns out that in 2D and in the absence of a high-k cutoff $\zeta_{\{\boldsymbol{k}\}}^{(1)}$ is a special case of a lattice sum first calculated by Lorenz [33] and Hardy [34], who showed that

$$\zeta_{\{k\}}^{(1)}(s) = \sum_{l_1,l_2}{}' \frac{1}{\left(l_1^2 + l_2^2\right)^s} = 4\zeta(s)\beta(s), \tag{38}$$

where the prime on the sum signifies that the value $l_1 = l_2 = 0$ must be omitted (for a derivation of Eq. (38), see [35]). Here, $\zeta(s) = \sum_{k=1}^{\infty} k^{-s}$ is the Riemann ζ function and $\beta(s) = \sum_{l=0}^{\infty} (-1)^l/(2l+1)^s$ is the Dirichlet β function. As already stated, (38) is undefined for $s = 1$ since the Riemann ζ function diverges; that is, the expectation of u cannot be calculated without a UV cutoff. For $s \geqslant 2$, that is, for all cumulants except the expectation, (38) is finite. The introduction of a high-k cutoff will only cause small deviations since the sums are infrared-dominated and we may write

$$\log q(\sigma) = i\sigma \langle u \rangle + 2 \sum_{s=2}^{\infty} \frac{(2i\sigma)^s}{s} \zeta(s)\beta(s), \tag{39}$$

where $\langle u \rangle$ is evaluated using a finite cutoff. The different UV behavior of the expectation and the higher-order cumulants has the consequence that the probability distribution for u is universal except for a cutoff-dependent shift. Thus, the variable $u - \langle u \rangle$ has values on the entire real axis. As long as the resulting probability distribution takes on negligible values

TABLE I. The first four relevant values of the Dirichlet β function.

s	2	3	4	5
$\beta(s)$	0.915 966	0.968 946	0.988 945	0.996 158

for values of u corresponding to visibilities outside the interval $[0,1]$, this does not create any inconsistency.

As pointed out by Bramwell in the context of the order-parameter distribution for the 2D XY model in the low-temperature limit [36], (39) is closely related to the Gumbel distribution

$$p_{\mathrm{G}}(x) = \exp[-(x+\gamma) - e^{-(x+\gamma)}] \tag{40}$$

(with the Euler constant $\gamma = 0.577\ldots$), which determines the statistics of the interference contrast for weakly interacting 1D Bose gases at zero temperature [7,8] (note that (40) is a normalized distribution with zero average and variance $\pi^2/6$). Its cumulant-generating function reads

$$\log p_{\mathrm{G}}(\sigma) = \sum_{s=2}^{\infty} \frac{(i\sigma)^s}{s} \zeta(s). \tag{41}$$

In fact, there are two nontrivial differences: (i) The presence of the Dirichlet β function in (39). This function rapidly converges to one so that it may be replaced by unity to a good approximation (see Table I). Since the expectation is nonuniversal anyway, this essentially amounts to increasing the variance by 9% or, equivalently, the width of the distribution by 4% (this may be seen as a convolution with a normalized Gaussian of appropriate width). (ii) The global factor of two which implies [accepting $\beta(s) \simeq 1$] that $q(u)$ is the convolution of two identical Gumbel distributions and $p(\mathcal{V}^2)$ its scaled mirror image. Thus, there is a striking similarity between the 2D case at finite temperature discussed here and the 1D case at vanishing temperature. However, owing to the different corresponding eigenspectra, passing from the latter to the former case does not amount to the simple replacement $K \mapsto 1/2\eta$, as suggested in [9].

The evolution of the distribution $q(u)$ with decreasing temperature, obtained numerically, is shown in Fig. 2. For simplicity, we have subtracted the nonuniversal expectation so that all distributions are centered around zero. The numerical data were obtained by generating 100 000 random surfaces per curve using a total of 1000 modes on a 16 000-point grid and then calculating $\mathcal{V}^2$ using Eqs. (20) and (21) without any approximation beyond the replacement of $\coth(\beta\omega_\lambda/2)$ with $2T/\omega_\lambda$. In particular, there is no expansion of $\exp(ih)$ to second order in h. For sufficiently low temperatures, the distribution approaches the universal low-temperature distribution, whose characteristic function is given in Eq. (39). The numerically calculated distribution for $n_{\mathrm{s}}/mT = 2/\pi$ should, of course, not be taken seriously: While the superfluid density remains finite at the critical point, the range of momenta where the quantum hydrodynamic action (12) is valid approaches zero. A proper result for the distribution of the interference contrast near T_c requires calculating the full counting statistics of the condensate number near the BKT transition, as is discussed in Sec. V.

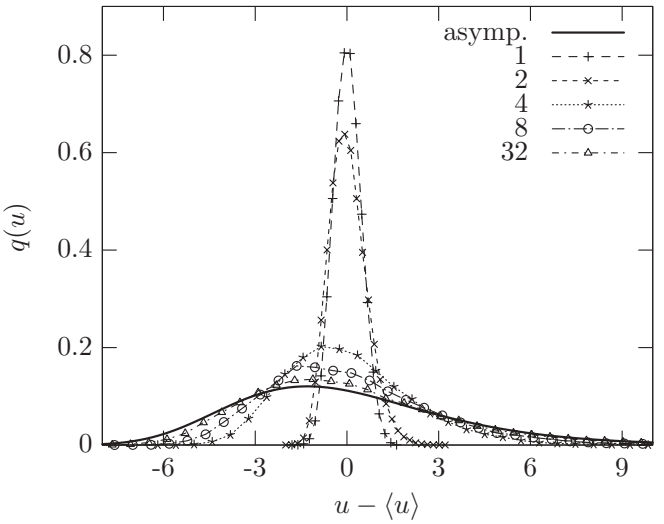

FIG. 2. Numerically calculated distributions $q(u - \langle u \rangle)$ for $T_c/T = 1,2,4,8,32$ (symbols, cf. legend) and a convolution of two Gumbel distributions (continuous line). The lines are a guide for the eye. Here and in the following plots, the statistical error is of the order of the symbol size.

As one can see in Fig. 3, the actual shape of the distribution that is obtained from scaling $q(u)$ by its standard deviation $\sqrt{\langle u^2 \rangle_c}$ is already quite close to the asymptotic result for $n_{\mathrm{s}}/mT = 2/\pi$ and converges rapidly with decreasing temperature.

B. Strongly anisotropic rectangle

While there is no general closed-form expression for $\zeta^{(a)}_{\{k\}}$ for arbitrary values of a, it is nonetheless possible to obtain an analytical expression for $p(\mathcal{V}^2)$ in the limiting case

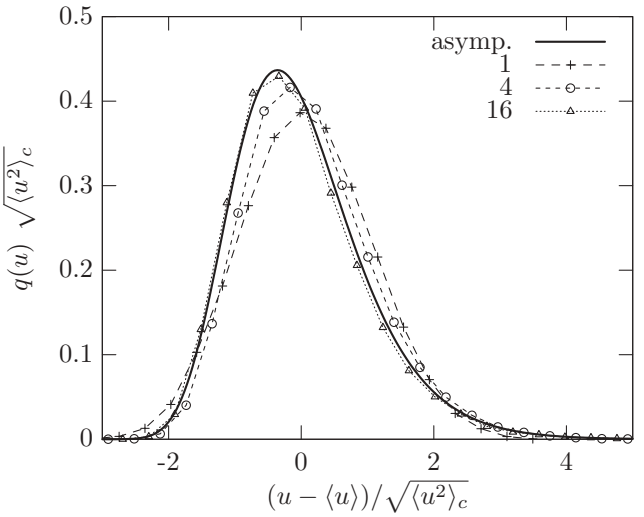

FIG. 3. The same data as in the previous figure (except for the choice of shown temperatures), but with normalized variance. In this representation, the convergence toward the asymptotic shape is considerably faster.

$a \ll 1$, that is, for a very anisotropic sample. The reason lies in the mathematical structure of the cumulants: Except for the nonuniversal expectation, all cumulants are given by sums which are dominated by the lowest-lying eigenvalues. Already for moderate values of the aspect ratio a (around 1/5; preliminary experimental data has been taken for aspect ratios even lower, $\lesssim 0.1$ [17]), the contribution of the modes along the shorter direction of the samples becomes negligible and one obtains

$$\zeta_{\{k\}}^{(a\ll 1)}(s) \simeq \sum_{l\neq 0} \frac{1}{l^{2s}} = 2\zeta(2s). \tag{42}$$

It is important to keep in mind that in order to remain in the 2D regime, the aspect ratio must not become too small; that is, Eq. (42) holds under the condition that $a \ll 1$, but at the same time $\hbar^2/m(aL)^2 < \mu, T$. If the second inequality is violated, the system becomes effectively 1D. At the same time, ϵ as given in Eq. (22) ceases to be a small parameter so that one can no longer justify the approximate treatment of $e^{i\phi(\boldsymbol{r})}$. However, we emphasize that Eq. (42) is well satisfied (for $s \geqslant 2$) already for moderately small a so that the strongly anisotropic 2D regime is well defined.

Substituting (42) into Eq. (32) yields

$$\begin{aligned}\log q(\sigma) &= i\sigma\langle u\rangle + \sum_{s=2}^{\infty} \frac{(2i\sigma)^s}{s}\zeta(2s) \\ &= i\sigma\left(\langle u\rangle - \frac{\pi^2}{3}\right) + \log[\Gamma(1-\sqrt{2i\sigma}) \\ &\quad \times \Gamma(1+\sqrt{2i\sigma})],\end{aligned} \tag{43}$$

or (defining $u_{\min} \equiv \langle u\rangle - \pi^2/3$)

$$q(\sigma) = \pi\sqrt{2i\sigma}\,\csc(\pi\sqrt{2i\sigma})e^{i\sigma u_{\min}}. \tag{44}$$

This function is meromorphic in the entire complex plane since the branch cuts of the square roots before and inside the cosecant cancel each other. This makes it possible to explicitly calculate its inverse Fourier transform $q(u) = (2\pi)^{-1}\int_{-\infty}^{\infty} d\sigma q(\sigma)e^{-iu\sigma}$ using the residue theorem. In the upper half plane, $q(\sigma)$ has no poles and falls off as $\exp[-\sqrt{2\mathrm{Im}(\sigma)}]$ for large arguments. Thus, for $u - u_{\min} \leqslant 0$, one may close the integration contour with a half-circle over the upper half plane and the integral vanishes. For $u - u_{\min} > 0$, one must close the contour in the lower half plane where $q(\sigma)$ has an infinite number of poles $\sigma_n = -in^2/2$. There, $e^{-i\sigma(u-u_{\min})}q(\sigma)$ has the residues $R_n = (-1)^{n-1}in^2e^{-n^2(u-u_{\min})/2}$. Thus, we obtain

$$q(u) = \begin{cases} 0 & u \leqslant u_{\min} \\ \sum_{n=1}^{\infty}(-1)^{n-1}n^2 e^{-\frac{n^2}{2}(u-u_{\min})} & u > u_{\min} \end{cases} \tag{45}$$

This can be written in a more compact form in terms of its cumulative distribution function,

$$q(u) = \theta(u - u_{\min}^{+})\frac{d}{du}\vartheta_4(e^{(u-u_{\min})/2}), \tag{46}$$

where θ is the Heaviside function, and $\vartheta_4(z) = 1 + 2\sum_{n=1}^{\infty}(-1)^n z^{n^2}$ is a Jacobi theta function. As a shorthand, we refer to the distribution described by Eq. (45) as the "Jacobi distribution."

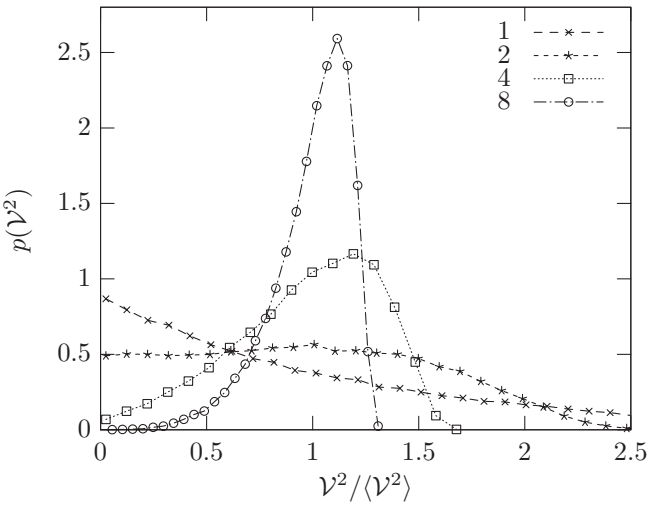

FIG. 4. Probability distributions $p(\mathcal{V}^2)$ of the visibility as a function of $\mathcal{V}^2/\langle\mathcal{V}^2\rangle$ for $T_c/T = 1,2,4,8$, for an anisotropy $a = 1/10$. Unlike the distribution in the isotropic case, the distribution for a strongly anisotropic sample undergoes strong shape modifications as T_c/T increases.

The evolution of the probability distribution with decreasing temperature in the strongly anisotropic case is shown in Fig. 4 (for $a = 1/10$). Unlike the isotropic case, the value $\mathcal{V}^2 = 0$ is actually quite probable at temperatures close to the critical point so that the shape of the distribution shows a clear qualitative change as the temperature is lowered toward the asymptotic regime. This observation is in qualitative agreement with preliminary experimental data taken at ENS [17]. Note that as long as the probability for a vanishing visibility stays finite, the shape of the distribution depends on the expectation and is thus explicitly cutoff dependent. However, since this dependence is only logarithmic, we expect the qualitative evolution of the shape to be insensitive to the precise value of the cutoff.

In turn, Fig. 5 shows the evolution of the probability distribution in the asymptotic low-temperature regime ($T = T_c/256$) with changing aspect ratio, confirming our earlier statement that the strongly anisotropic regime is reached already for $a \lesssim 1/5$.

C. Harmonically trapped sample

As we have pointed out in the preceding discussion, the cumulants (and hence the shape of the distribution) are dominated by the excitations with the lowest frequency. The periodic boundary conditions we have used up to this point are thus quite artificial: Even for a homogeneous system, going over to different boundary conditions will have effects on the shape of the distribution (see [9] for examples). However, the differences are mere numerical factors appearing in the cumulants (for an example, the variance in a 3D homogeneous sample is smaller by a factor of 1.67 when Dirichlet boundary conditions are used instead of periodic ones [37]); the dependence on physical parameters remains unaltered.

We now consider the geometry most relevant for actual experiments: a sample which is harmonically trapped. For

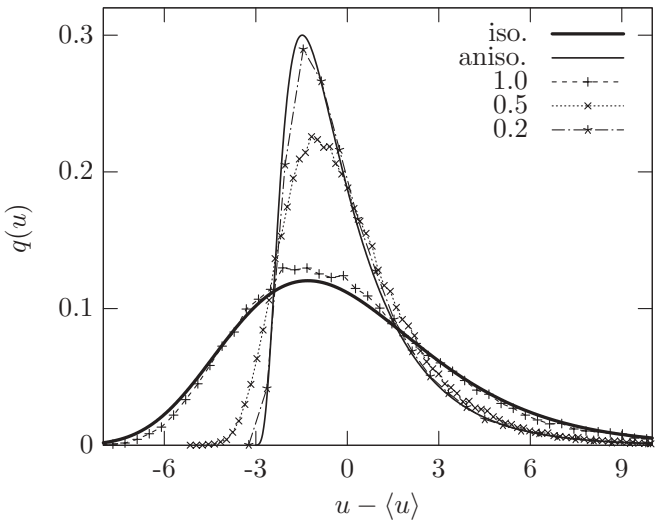

FIG. 5. Probability density $q(u)$ for $a = 1, 1/2, 1/5$, as well as the asymptotic distributions for the isotropic (heavy line) and strongly anisotropic (thin line) regime. For $a \leqslant 1/10$ (not shown), the results become indistinguishable from the strongly anisotropic limiting case. A value of $T_c/T = 256$ has been chosen to ensure that the distributions are well within the asymptotic low-temperature regime.

simplicity, we consider an isotropic trap with trapping frequency ω. If the particle number is large enough to warrant $N\tilde{g} \gg 1$ [6] (which is readily fulfilled for $\tilde{g} \sim 0.1$ and $N \sim 10^3$) and the temperature is sufficiently low, the density distribution takes the form of a Thomas-Fermi profile:

$$\bar{n}(r) = \bar{n}(0)\left[1 - \left(\frac{r}{R}\right)^2\right]\theta(R-r); \quad R = \sqrt{\frac{2g\bar{n}(0)}{m\omega^2}}. \tag{47}$$

In the following, we assume the entire sample is superfluid and we need not distinguish between the superfluid and the total density. This requires the temperature to be substantially below $T_{\mathrm{BKT}} = (4\pi N\omega^2/\tilde{g}D_c^2)^{1/2}$ where the phase space density $D = \bar{n}\lambda_T^2$ reaches the critical value $D_c = \log(380/\tilde{g})$ of the BKT transition in the trap center [38]. Moreover, we want to be in the regime of near-unity visibility so that we must fulfill $\delta\phi(R) = [\bar{n}(0)\lambda_T^2]^{-1}\log(R^2/\xi^2) \ll 1$ [6] or, equivalently,

$$T \ll T_\phi = \frac{1}{\log(2\tilde{g}N/\pi)}\sqrt{\frac{4\pi N\omega^2}{\tilde{g}}}. \tag{48}$$

For $N = 5000$, $\tilde{g} = 0.1$, and $\omega = 2\pi \times 20$ Hz, one obtains $T_{\mathrm{BKT}} = 95$ nK and $T_\phi = 132$ nK (for lower interaction constants, both are even higher) so that the low-temperature regime we are considering is within experimental reach.

In analogy to the calculation of the low-energy modes in 3D [39], the solutions $\psi_{n,l}(r,\theta)$ of the Euler-Lagrange equation (16) with open boundary conditions yield the frequencies

$$\omega_{n,l} = \omega\sqrt{\frac{n(n+2) - l^2}{2}}. \tag{49}$$

Here, $n = 0,1,2\ldots$ is a radial and $l = -n, -n+2, \ldots, n-2, n$ is an azimuthal index [40]. The eigenmodes are of the general form,

$$\psi_{n,l}(r,\theta) = \frac{P_{n,|l|}(r/R)}{R} \times \begin{cases} \cos(l\theta)/\sqrt{\pi} & l > 0 \\ 1/\sqrt{2\pi} & l = 0 \\ \sin(|l|\theta)/\sqrt{\pi} & l < 0 \end{cases}, \tag{50}$$

where $P_{n,|l|}(x) = \sum_k a_k^{(n,|l|)} x^k$ are polynomials, the coefficients of which may be obtained from the recursion relation

$$a_{k+2}^{(n,|l|)}[l^2 - (k+2)^2] = a_k^{(n,|l|)}[n(n+2) - k(k+2)]. \tag{51}$$

Hence, the $P_{n,|l|}(x)$ are either even or odd, and the highest and lowest occurring powers of x are n and $|l|$, respectively. The magnitude of the lowest coefficient is fixed by the normalization condition $\int_0^1 dx\, x\, P_{n,|l|}(x)^2 = 1$.

The eigenmodes satisfy the orthogonality relations

$$\int_0^{2\pi} d\theta \int_0^R dr\, r\, \psi_{n,l}(r,\theta)\psi_{n',l'}(r,\theta) = \delta_{n,n'}\delta_{l,l'} \tag{52}$$

on a disk of radius R. For different l, the orthogonality is assured by the azimuthal part, for equal l, by the radial part of the eigenfunctions.

A particularly important subset of the eigenfunctions is formed by the *surface modes*

$$\psi_{n,\pm n}(r) = \sqrt{2(n+1)}\frac{r^n}{R^{n+1}} \begin{cases} \cos(n\theta)/\sqrt{\pi} & l = n, \\ \sin(n\theta)/\sqrt{\pi} & l = -n, \end{cases} \tag{53}$$

with eigenfrequencies $\omega_{n,\pm n} = \sqrt{n}\omega$. By inspecting Eq. (49), one finds that most of the lowest-lying modes are such surface modes. This is physically intuitive, since the phase stiffness as given by Eq. (47) is lower close to the rim so that low-energy excitations should live on the boundary of the sample. It is thus to be expected that the condensate fraction and hence the interference contrast is dominated by the behavior of the surface modes.

If we substitute the eigenmodes and eigenfrequencies of the surface modes into the definitions of ϵ and u, we obtain [noting that $\psi_{n,l}(\boldsymbol{r})^2/\omega_{n,l}^2$ takes its maximum for $|l| = 1$ and $r = R$]:

$$\epsilon^2 = \frac{4}{\pi}\frac{mT}{n_{\mathrm{s}}(0)}; \quad u = \pi\frac{n_{\mathrm{s}}(0)}{mT}(1 - \mathcal{V}^2). \tag{54}$$

Once again, as in the homogeneous case, there is no explicit dependence on the interaction constant. However, in the present case, there is an *implicit* dependence on the interaction constant since the latter defines the geometry of the sample and the density in the center is given by $\bar{n}(0) = mN\omega^2/\pi g$.

Carrying out the expansion (27), we find that in the case of harmonic trapping, the integrals (28) become nontrivial. One readily finds that $I_{n,l,n',l'} = \delta_{l,l'}I_{n,n'}(|l|)$ and $J_{n,l} = \delta_{l,0}J_n$, which follows immediately from the azimuthal part of the eigenfunctions. This shows already that there is no I that "couples" different surface modes (they all differ in l) and no J that involves any surface modes. The diagonal elements for the surface modes are readily found to be $I_{n,\pm n}(n) = 2/(n+2)$. On closer inspection, one finds that the matrices $I_{n,n'}(|l|)$ are tridiagonal in the sense that they are nonvanishing only for

TABLE II. Variance and standard deviation of u in the harmonically trapped case, exact and in two different approximations.

Approximation	$\langle u^2\rangle_c$	$\sqrt{\langle u^2\rangle_c}$
Exact	2.813	1.677
Diagonal	2.496	1.580
Surface	2.160	1.470

$n' = n, n \pm 2$ (we recall that n and l are either both even or both odd); likewise, only $J_2 = 1/\sqrt{3}$ is finite.

Taken together with the physical intuition that the statistics should be dominated by the surface modes, these results suggest that it should be a reasonable approximation to disregard J_2 and the nondiagonal elements of the matrices $I_{n,n'}(|l|)$, which would make it possible to carry out the integration leading to Eq. (31). In order to see whether this leads to correct results, we evaluate the variance of u first exactly, then in the "diagonal" approximation. A straightforward calculation gives

$$\langle u^2\rangle_c = 2{\sum_{n,n',l}}' \frac{I_{n,n'}(|l|)^2}{\tilde{\omega}_{n,l}^2\tilde{\omega}_{n',l}^2} - \frac{1}{6}{\sum_{n}}' \frac{I_{2,n}(0)}{\tilde{\omega}_{n,0}} + \frac{1}{72}, \tag{55}$$

which is reminiscent of a structurally similar expression for the variance of condensate fluctuations in a 3D harmonic trap by Giorgini *et al.* [41], but with two additional terms which come from the finiteness of J_2. Once again, the primes on the sums are reminders that the sums go only over permitted values of the indices.

In Table II, we give the numerical value of Eq. (55) calculated in three different manners: first exactly, that is, without approximations apart from the numeric calculation, and in two different approximations. In the "diagonal" approximation, we disregard the two last terms which are generated by J_2 and take into account only the diagonal elements of $I_{n,n'}(|l|)$ in the first term. The "surface" approximation goes even one step further by dropping all contributions except those coming from the surface modes. We see that the diagonal approximation is quite satisfactory (we recall that the higher cumulants are increasingly dominated by the lowest-lying modes so that we expect the approximation to improve with increasing cumulant order) and even the elementary surface approximation fares reasonably well.

In the diagonal approximation, u reads

$$u = {\sum_{n,l}}' \frac{t_{n,l}^2}{\tilde{\omega}_{n,l}^2} I_{n,n}(|l|), \tag{56}$$

and the spectral ζ function is

$$\zeta_{\{n,l\}}(s) = {\sum_{n,l}}' \left(\frac{I_{n,n}(|l|)}{\tilde{\omega}_{n,l}^2}\right)^s. \tag{57}$$

In the surface approximation, this can be written explicitly as

$$\zeta_{\{n\}}^{(\mathrm{surf})}(s) = 2\sum_{n=1}^{\infty}\left(\frac{2}{n(n+2)}\right)^s \approx 2\left(\frac{2}{3}\right)^s \zeta(3s/2). \tag{58}$$

The approximation on the right-hand side is better than within 1% for all $s \geqslant 2$. The global factor of 2 comes from the twofold degeneracy of the surface modes. As in the strongly anisotropic rectangle case, it compensates the global factor of $1/2$ in Eq. (32).

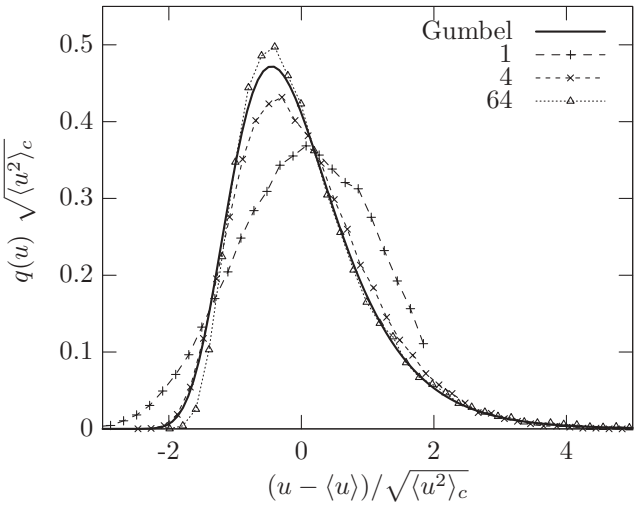

FIG. 6. Scaled distribution $q(u)$ for the harmonically trapped case, for $T_c/T = 1,4,64$. A Gumbel distribution (not a convolution of Gumbel functions) scaled to have unit variance is shown for comparison (continuous line). The sharp falloff at the right end of the $T = T_c$ curve corresponds to zero visibility, while the $T = T_c/64$ curve is already well within the asymptotic low-temperature regime. Quite amusingly, the profile for $T = T_c/T = 16$ (not shown) comes out almost superposed with a Gumbel distribution while the asymptotic distribution comes quite close to it, but remains more sharply peaked, in agreement with the arguments presented in the text.

While it does not seem possible to derive a closed-form expression for the associated probability distribution, the form of the spectral ζ function suggests that the distribution should be something intermediate between a Gumbel distribution [where the spectral ζ function is proportional to $\zeta(s)$] and a Jacobi distribution [where the spectral ζ function is proportional to $\zeta(2s)$], that is, more asymmetric than the former, but less asymmetric than the latter. Of course, the contributions from the neglected modes will render the actual distribution somewhat more symmetric than this argument suggests, but it should remain qualitatively valid. This is supported by numerical results which are calculated without approximations, as can be seen in Fig. 6.

V. DISTRIBUTION AT THE CRITICAL POINT

A quite interesting aspect associated with the statistics of interference amplitudes is the possibility of measuring the universal probability distribution of the order parameter near a critical point. Indeed, as has been shown in Sec. II, the visibility is identical with the condensate fraction provided the integration length is much larger than the interparticle spacing. Our calculation of the resulting visibility distribution in the previous section is valid deep in the Bose-condensed regime, where the visibility is close to one.

In the following, we discuss the situation close to the critical point of Bose-Einstein-condensation, that is, in a regime where

the system size L is large compared to microscopic lengths but of the same order or smaller than the correlation length ξ of the infinite system. Mathematically, this may be expressed by a dimensionless parameter,

$$x = tL^{1/\nu} = \pm\left(\frac{L}{\xi}\right)^{1/\nu} = \mathcal{O}(1), \tag{59}$$

that measures the deviation from the critical point due to the finite system size. Here $t = (T - T_c)/T_c$ is the dimensionless distance from the bulk critical temperature T_c and $\nu \approx 0.672$ the critical exponent that characterizes the divergence $\xi \sim |t|^{-\nu}$ of the correlation length in a 3D Bose-Einstein condensate (BEC) [42,43]. This exponent has, in fact, been measured also in dilute ultracold gases [44]. Quite generally, finite size scaling predicts that the probability distribution of a two-component order parameter $\boldsymbol{s}$ (for a BEC, $\boldsymbol{s}^2 = n_0$ is the condensate fraction) in the critical regime has a scaling form [13,45]

$$p(\boldsymbol{s},t,L) = L^{2y} p_d^\star(\boldsymbol{s}L^y, tL^{1/\nu}). \tag{60}$$

Here

$$y(d) = (d - 2 + \eta)/2 \tag{61}$$

is related to the standard anomalous dimension η of the XY model while $p_d^\star(z,x)$ is a universal, non-Gaussian distribution that only depends on $z^2 = n_0 L^{2y}$. The existence of such a distribution for properly scaled block-spin variables $\boldsymbol{s}L^y$ with finite moments of arbitrary order, is, in fact, a basic assumption of the renormalization group approach to critical points, as emphasized by Parisi [46]. Precisely at the critical point, where $x = 0$, the distribution is determined by the effective potential $V_{\rm eff}^\star(z)$ of the underlying field theory at the fix point via

$$p_d^\star(z,x=0) \sim \exp[-V_{\rm eff}^\star(z)]. \tag{62}$$

Within the standard two-component Φ^4 theory, the distribution $p_3^\star(z,x)$ in the 3D case has been calculated by Chen *et al.* [47], taking into account the singularities associated with the Goldstone mode. The resulting distribution at the critical point $x = 0$ is shown in Fig. 7. It exhibits a maximum at $z^2 \simeq 1.146$. The most probable value for the number of particles in the condensate therefore scales as $\bar{N}_0 \simeq L^{2-\eta}$, which is subextensive, as expected right at T_c. The average typical visibility,

$$\sqrt{\langle \mathcal{V}^2 \rangle} \sim 1/L^{1+\eta}, \tag{63}$$

at the critical point will therefore vanish with an anomalous power of the integration length L, that is, basically like $1/L$ because $\eta \simeq 0.03$ is rather small. Moreover, the fact that the variance of the variable z^2 is a universal constant of order one, the so-called Binder cumulant [45], implies that the fluctuations of the visibility scale with the same anomalous power of the integration length as the average.

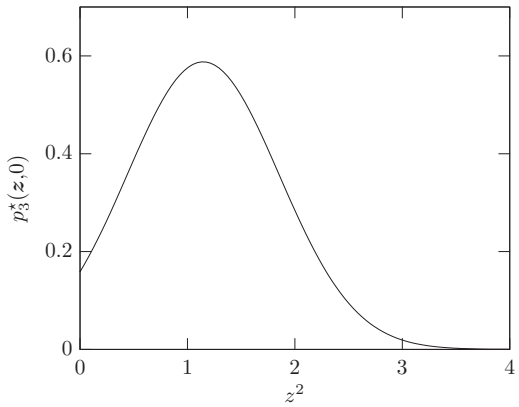

FIG. 7. The universal distribution $p_3^\star(z,0)$ for the order parameter z in 3D directly at the critical point as calculated in [47].

In the 2D case, there is no breaking of a continuous symmetry at finite temperature. Instead, there is a BKT transition to quasi-long-range order below T_c, where the gas is a proper superfluid but not a BEC. The absence of a finite correlation length below T_c in this case does not allow to define a simple analog of the variable x in (59). Right at the BKT transition, however, one expects again a universal order-parameter distribution function $p_2^\star(z)$ for the variable $z^2 = n_0 L^\eta$, since $y = \eta/2$ in 2D. In contrast to the situation discussed in Sec. IV, where the distribution of the interference contrast has been calculated deep in the superfluid regime and the visibility is close to one, the distribution $p_2^\star(z)$ with its anomalous scaling applies to 2D Bose gases whose size is much larger than the phase coherence length ℓ_ϕ. The thermal phase fluctuations then imply an average condensate fraction $\langle n_0 \rangle \sim L^{-\eta}$ which decreases with system size. The typical value $\sqrt{\langle \mathcal{V}^2 \rangle} \sim L^{-\eta}$ of the visibility is therefore close to zero. In fact, since the 2D superfluid phase corresponds to a line of critical points at *any* $T < T_c$, this behavior of the average visibility is valid at *arbitrary* temperature below T_c in the limit $L \to \infty$ with a temperature-dependent exponent $\eta(T)$, which reaches its critical value $\eta_c = 1/4$ at T_c. Note that, independent of the precise form of the distribution $p_2^\star(z)$, the very existence of a scaling variable $z^2 = n_0 L^\eta$ immediately implies the subextensive scaling $\langle N_0 \rangle \sim L^{2-\eta}$ of the average number of particles in the condensate for an interacting 2D Bose gas and its anomalous fluctuations $\mathrm{Var} N_0 \sim \langle N_0 \rangle^2$ [48] in the thermodynamic limit.

In order to observe this anomalous scaling, the system size must be large compared to the phase coherence length, $L \gg \ell_\phi = \xi e^{1/2\eta(T)}$. At the critical point, this is readily fulfilled for typical system sizes of the order of some 10 μm and healing lengths of the order of 0.1 μm. By contrast, for $T \ll T_c$, the system size required to be in the anomalous scaling regime rapidly exceeds experimentally feasible values. Therefore, one has $L \ll \ell_\phi$ in practice and the visibility distribution can be determined by an expansion around $\mathcal{V}^2 \approx 1$, as done in Sec. IV.

VI. CONCLUSION

In conclusion, we have shown that interference experiments may be used as a direct measurement of the statistics of the condensate fraction in ultracold Bose gases. Unlike in interference experiments in classical optics, where the fringe visibility is determined by a deterministic cross correlation

function of the optical fields [49,50], the interference contrast of matter waves is a quantum observable. Repeated experiments with identically prepared condensates therefore produce a statistical distribution of values instead of a reproducible single value. The resulting distributions are non-Gaussian even in the thermodynamic limit and have been calculated explicitly for 2D Bose gases at temperatures such that their effective condensate fraction is close to one. Quite generally, the interference contrast is a self-averaging observable in situations with long-range phase coherence. Our findings for the 2D strongly anisotropic case are in qualitative agreement with preliminary data taken at ENS [17]. Clearly, a quantitative comparison between theory and experiment is needed to verify our predictions. In particular, the interference statistics might be used as a precise thermometer of the gases, similar to what has been achieved in 1D gases [10]. A quite interesting open problem, from both a theoretical and an experimental point of view, is the analysis of the interference contrast near the transition to the normal phase. It offers the possibility of directly measuring the distribution of the order parameter[1] near the critical point, a quantity that is very hard to measure otherwise.

ACKNOWLEDGMENTS

The authors acknowledge helpful discussions with M. Holzmann and B. Spivak. We are very grateful to Z. Hadzibabic, P. Krüger, and J. Dalibard for providing us with unpublished experimental data [17]. Part of this work has been supported by the DFG research unit "Strong Correlations in Multiflavor Ultracold Quantum Gases."

APPENDIX A: UNIVERSAL SCALING IN 3D

As shown in Sec. II, the distribution of the condensate number, which is related to the intensive two-component vector order parameter $\boldsymbol{s}$ that describes Bose-Einstein condensation from the point of view of statistical physics by $N_0 = L^3 s^2$ is not a simple Gaussian. This is a result of the fact that in the case where the broken symmetry is continuous, the order-parameter correlation length is infinite for all temperatures below T_c [37]. The universal distribution function of the condensate number below T_c is, in fact, contained in the result (32) for the logarithm of the characteristic function of the random variable $u = 2(1-\mathcal{V}^2)/\epsilon^2$. In 3D, the small parameter ϵ defined in Eq. (25) can be written in the form

$$\epsilon^2 = \frac{1}{\pi^2}\frac{\xi_J(T)}{L}, \tag{A1}$$

where we have introduced the Josephson length $\xi_J = mT/n_s$. For any finite temperature, therefore, ϵ goes to zero for a system size L much larger than the Josephson length. The universal distribution $p(u)$ for the fluctuating variable,

$$u = \frac{2\pi^2 L}{\xi_J}\left(1 - \frac{N_0^2}{N^2}\right), \tag{A2}$$

which determines the distribution of the condensate number of a 3D BEC below T_c, is fixed by the exact cumulants given in (33). It depends on the 3D spectral ζ function

$$\zeta_{\{\lambda\}}(s) = {\sum_{l_1,l_2,l_3}}' \frac{1}{\left(l_1^2 + l_2^2 + l_3^2\right)^s} = \sum_{n=1}^{\infty} \frac{A_3(n)}{n^s}, \tag{A3}$$

for which, unfortunately, no closed-form expression seems to exist [35]. It is evident, however, that $\zeta_{\{\lambda\}}(s)$ is convergent for all $s > 3/2$ and thus all cumulants except the first are finite. The variable with a proper, non-Gaussian distribution in the limit $L \to \infty$ is thus $n_0^2 L/\xi_J$, which implies that the condensate fraction is a self-averaging variable. Its fluctuations, however, are not of order $1/\Omega$ as usual but only decay like $1/L^2$ [37]. Since all higher cumulants including the variance are finite and have the same scaling with system size L, the ratios $\langle u^s\rangle_c/\langle u^2\rangle_c^{s/2}$ are constant and finite. A special case of this result has in fact been found by Kocharovsky *et al.* [51], who calculated the cumulants of the number of condensed atoms in a 3D BEC within a Bogoliubov approach. In particular, to leading order in ϵ, our cumulants from Eq. (34) agree with theirs, showing the close connection between the condensed fraction and the interference amplitude.

APPENDIX B: THE 1D CASE AT ZERO TEMPERATURE

In this appendix, we discuss the case of a homogeneous 1D Bose gas at vanishing temperature. Using $c = \sqrt{g n_s/m}$ and substituting $n_s/m = cK/\pi$, where K is the dimensionless Luttinger parameter, the hydrodynamic action (12) governing the phase difference $\phi = \varphi_2 - \varphi_1$ of two interfering 1D Bose gases has the form

$$S_0[\phi] = \frac{K}{4\pi c}\int_0^L \mathrm{d}x \int_0^\beta \mathrm{d}\tau\{[\partial_\tau\phi]^2 + c^2[\partial_x\phi]^2\}, \tag{B1}$$

where we have kept β finite. Using the Fourier expansion,

$$\phi(x,\tau) = \frac{1}{\sqrt{\beta L}}\sum_k \sum_{n=-\infty}^{\infty} \phi_k(\omega_n) e^{i(kx-\omega_n\tau)}, \tag{B2}$$

where $k = 2\pi l/L$ with $l \in \mathbb{Z}$, and $\omega_n = 2\pi n/\beta$ are the bosonic Matsubara frequencies, the action takes the diagonal form:

$$S_0[\phi] = \frac{K}{4\pi c}\sum_{k,n}\left(c^2k^2 + \omega_n^2\right)|\phi_k(\omega_n)|^2. \tag{B3}$$

The generating function $p(\sigma) = \langle e^{i\sigma\mathcal{V}^2}\rangle$ for the square of the visibility requires calculating a functional integral with a perturbation

$$S_1 = \frac{i\sigma}{N^2}\int dx \int dx' \bar{n}(x)\bar{n}(x')\cos[\phi(x) - \phi(x')] \tag{B4}$$

to the action (B1). This perturbation only contains the phase difference $\phi(x) \equiv \phi(x,0)$ on the boundary in imaginary time τ. Except for $\phi(x) = \phi(x,\tau = 0)$, all variables are therefore Gaussian and can be integrated out. The problem then is completely analogous to that of backscattering from

[1]Note that for 2D gases there is no true order parameter, yet there is a nontrivial distribution of the number of particles at zero momentum.

a single impurity in a Luttinger liquid discussed by Kane and Fisher [52].

Upon elimination of the modes $\phi_k(\tau \neq 0)$, one obtains the reduced free action

$$S_0[\phi] = \frac{K}{2\pi} \sum_{k=-\Lambda}^{\Lambda} |k|\,|\phi(k)|^2 \tag{B5}$$

for the remaining, non-Gaussian degrees of freedom, where we have explicitly written the ultraviolet cutoff Λ. This corresponds to a *nonlocal* action in space of the form

$$S_0[\phi(x)] = \frac{\alpha}{8\pi^2} \int dx \int dx' \left(\frac{\phi(x) - \phi(x')}{x - x'}\right)^2 \tag{B6}$$

that arises in τ space for dissipative quantum mechanics of a single particle [53] or in the study of nontrivial ground states of open strings [54]. Equations (B5) and (B6) are equivalent if the associated dimensionless strength α of the dissipation is related to the Luttinger parameter by $\alpha = 2K$.

Following the arguments of Sec. IV, the distribution of the interference contrast can be calculated analytically in the limit $\epsilon^2 = 1/K \ll 1$ by expanding S_1 in Eq. (B4) to second order in ϕ. Again, it is then natural to consider the characteristic function $q(\sigma) = \langle e^{i\sigma(1-\mathcal{V}^2)} \rangle$ which corresponds to a perturbation (for a homogeneous system with $\bar{n}(x) = N/L$):

$$\hat{S}_1[\phi] = -\frac{i\sigma}{2L^2} \int dx \int dx' [\phi(x) - \phi(x')]^2. \tag{B7}$$

Substituting the Fourier series representation for $\phi(x)$, this becomes

$$\hat{S}_1[\phi] = -\frac{i\sigma}{L} \sum_{k\neq 0} |\phi_k|^2. \tag{B8}$$

The functional integral is now Gaussian and can be evaluated exactly, giving

$$q(\sigma) = \prod_{k>0} \left(1 - \frac{2\pi i\sigma}{KkL}\right)^{-1}, \tag{B9}$$

or

$$\log q(\sigma) = \frac{i\sigma}{K} \langle 1 - \mathcal{V}^2 \rangle + \sum_{s=2}^{\infty} \frac{1}{s} \left(\frac{i\sigma}{K}\right)^s \zeta(s), \tag{B10}$$

where again the expectation is explicitly cutoff dependent. Comparison with Eq. (40) shows that the variable $K(\langle \mathcal{V}^2 \rangle - \mathcal{V}^2)$ has a Gumbel distribution of the normalized form given in Eq. (40), as derived in [8].

Note that the action $S_0 + S_1$, as given by Eqs. (B1) and (B4), differs from the action of the boundary sine-Gordon model that appears for dissipative quantum mechanics in a (purely imaginary) periodic potential. Instead, it corresponds to a classical 1D XY model with infinite range interactions. However, a mapping to a sine-Gordon model (relying on a Hankel transform rather than a Fourier transform of the probability distribution) is possible in the thermodynamic limit and has been used by Gritsev *et al.* in [7] to calculate the distribution function of the interference contrast for *arbitrary* values of the Luttinger parameter K.

[1] M. R. Andrews, C. G. Townsend, H.-J. Miesner, D. S. Durfee, D. M. Kurn, and W. Ketterle, Science **275**, 637 (1997).

[2] Z. Hadzibabic, P. Krüger, M. Cheneau, B. Battelier, and J. Dalibard, Nature (London) **441**, 1118 (2006).

[3] S. Hofferberth, I. Lesanovsky, B. Fischer, T. Schumm, and J. Schmiedmayer, Nature (London) **449**, 324 (2007).

[4] D. S. Petrov, M. Holzmann, and G. V. Shlyapnikov, Phys. Rev. Lett. **84**, 2551 (2000).

[5] D. S. Petrov, G. V. Shlyapnikov, and J. T. M. Walraven, Phys. Rev. Lett. **85**, 3745 (2000).

[6] For a review, see I. Bloch, J. Dalibard, and W. Zwerger, Rev. Mod. Phys. **80**, 885 (2008).

[7] V. Gritsev, E. Altman, E. Demler, and A. Polkovnikov, Nat. Phys. **2**, 705 (2006).

[8] A. Imambekov, V. Gritsev, and E. Demler, in *Proceedings of the Enrico Fermi Summer School on Ultracold Fermi Gases 2006*, edited by M. Inguscio, W. Ketterle, and C. Salomon (IOS Press, Amsterdam, 2007), p. 535.

[9] A. Imambekov, V. Gritsev, and E. Demler, Phys. Rev. A **77**, 063606 (2008).

[10] S. Hofferberth, I. Lesanovsky, T. Schumm, A. Imambekov, V. Gritsev, E. Demler, and J. Schmiedmayer, Nat. Phys. **4**, 489 (2008).

[11] For a discussion of counting statistics in the quite different context of transferred charges in the currents through mesoscopic devices, see Y. Nazarov and Y. Blanter, *Quantum Transport* (Cambdrige University Press, Cambridge, 2009).

[12] M. E. Fisher and M. N. Barber, Phys. Rev. Lett. **28**, 1516 (1972).

[13] E. Brézin and J. Zinn-Justin, Nucl. Phys. B **257**, 867 (1985).

[14] V. L. Berezinskii, Sov. Phys. JETP **34**, 610 (1971).

[15] J. M. Kosterlitz and D. J. Thouless, J. Phys. C **6**, 1181 (1973).

[16] N. R. Cooper and Z. Hadzibabic, Phys. Rev. Lett. **104**, 030401 (2010).

[17] Z. Hadzibabic, P. Krüger, and J. Dalibard (unpublished measurements).

[18] P. Krüger, Z. Hadzibabic, and J. Dalibard, Phys. Rev. Lett. **99**, 040402 (2007).

[19] A. Imambekov, I. E. Mazets, D. S. Petrov, V. Gritsev, S. Manz, S. Hofferberth, T. Schumm, E. Demler, and J. Schmiedmayer, Phys. Rev. A **80**, 033604 (2009).

[20] A. Polkovnikov, E. Altman, and E. Demler, Proc. Natl. Acad. Sci. **103**, 6125 (2006).

[21] D. S. Petrov, D. M. Gangardt, and G. V. Shlyapnikov, J. Phys. IV (France) **116**, 5 (2004).

[22] A. Polkovnikov, Europhys. Lett. **78**, 10006 (2007).

[23] P. C. Hohenberg, Phys. Rev. **158**, 383 (1967).

[24] N. D. Mermin and H. Wagner, Phys. Rev. Lett. **17**, 1307 (1966).

[25] Z. Hadzibabic and J. Dalibard, in *Nano Optics and Atomics: Transport of Light and Matter Waves*, edited by R. Kaiser and D. Wiersma (Enrico Fermi summer school, Varenna, 2009), Vol. CLXXIII.

[26] E. Freitag and R. Busam, *Complex Analysis* (Springer, Berlin, 2008), 2nd ed.

[27] D. S. Petrov and G. V. Shlyapnikov, Phys. Rev. A **64**, 012706 (2001).
[28] P. Cladé, C. Ryu, A. Ramanathan, K. Helmerson, and W. D. Phillips, Phys. Rev. Lett. **102**, 170401 (2009).
[29] J. I. Gillen, W. S. Bakr, A. Peng, P. Unterwaditzer, S. Fölling, and M. Greiner, Phys. Rev. A **80**, 021602 (2009).
[30] S. P. Rath, T. Yefsah, K. J. Günter, M. Cheneau, R. Desbuquois, M. Holzmann, W. Krauth, and J. Dalibard, Phys. Rev. A **82**, 013609 (2010).
[31] C.-L. Hung, X. Zhang, N. Gemelke, and C. Chin, e-print arXiv:1009.0016.
[32] N. Prokofev and B. Svistunov, Phys. Rev. A **66**, 043608 (2002).
[33] L. Lorenz, Mat. Tidsskr. **1**, 97 (1871).
[34] G. H. Hardy, Messenger Math **49**, 85 (1919).
[35] I. J. Zucker, J. Phys. A **7**, 1568 (1974).
[36] S. T. Bramwell, Nat. Phys. **5**, 444 (2009).
[37] W. Zwerger, Phys. Rev. Lett. **92**, 027203 (2004).
[38] N. Prokof'ev, O. Ruebenacker, and B. Svistunov, Phys. Rev. Lett. **87**, 270402 (2001).
[39] S. Stringari, Phys. Rev. Lett. **77**, 2360 (1996).
[40] T.-L. Ho and M. Ma, J. Low Temp. Phys. **115**, 61 (1999).
[41] S. Giorgini, L. P. Pitaevskii, and S. Stringari, Phys. Rev. Lett. **80**, 5040 (1998).
[42] M. Campostrini, M. Hasenbusch, A. Pelissetto, P. Rossi, and E. Vicari, Phys. Rev. B **63**, 214503 (2001).
[43] E. Burovski, J. Machta, N. Prokof'ev, and B. Svistunov, Phys. Rev. B **74**, 132502 (2006).
[44] T. Donner, S. Ritter, T. Bourdel, A. Öttl, M. Köhl, and T. Esslinger, Science **315**, 1556 (2007).
[45] K. Binder, Z. Phys. B **43**, 119 (1981).
[46] G. Parisi, *Statistical Field Theory* (Addison-Wesley, Reading, MA, 1988).
[47] X. S. Chen, V. Dohm, and N. Schultka, Phys. Rev. Lett. **77**, 3641 (1996).
[48] F. Meier and W. Zwerger, Phys. Rev. A **60**, 5133 (1999).
[49] F. Zernike, Physica **5**, 785 (1938).
[50] E. Wolf, *Introduction to the Theory of Coherence and Polarization of Light* (Cambdrige University Press, Cambridge, 2007).
[51] V. V. Kocharovsky, Vl. V. Kocharovsky, and M. O. Scully, Phys. Rev. A **61**, 053606 (2000).
[52] C. L. Kane and M. P. A. Fisher, Phys. Rev. B **46**, 15233 (1992).
[53] M. P. A. Fisher and W. Zwerger, Phys. Rev. B **32**, 6190 (1985).
[54] C. G. Callan and L. Thorlacius, Nucl. Phys. B **329**, 117 (1990).